Cell Reports, Volume *42*

Supplemental information

The stability of the myelinating oligodendrocyte transcriptome is regulated by the nuclear lamina

Mathilde Pruvost, Julia Patzig, Camila Yattah, Ipek Selcen, Marylens Hernandez, Hye-Jin Park, Sarah Moyon, Shibo Liu, Malia S. Morioka, Lindsay Shopland, Osama Al-Dalahmah, Jaroslav Bendl, John F. Fullard, Panos Roussos, James Goldman, Ye He, Jeffrey L. Dupree, and Patrizia Casaccia

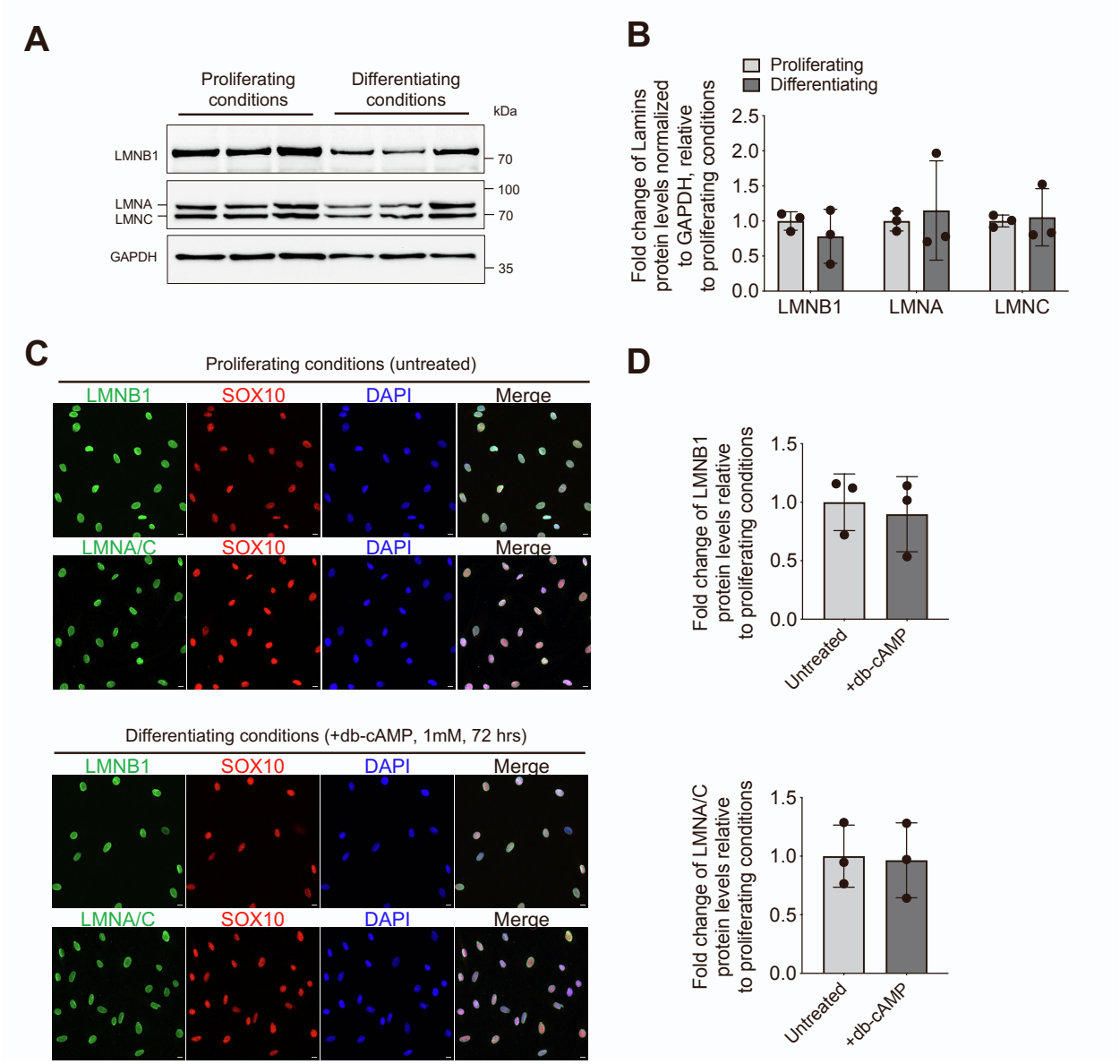

Supplemental Figure S1. Lamins are expressed in Schwann cells cultured in proliferating and differentiating conditions.

(A) Western blot of LMNB1 and LMNA/C protein levels in rat Schwann cells cultured in proliferating or differentiating conditions. GAPDH used as a loading control. Molecular weights indicated on the right (n = 3 independent cultures).

(B) Quantification of the protein levels of LMNB1, LMNA, LMNC relative to GAPDH. Data represent average ± SD, of 3 independent cultures for each condition ($p \geq 0.05$, two-way ANOVA).

(C) Representative confocal image of rat Schwann cells cultured in proliferating or differentiating conditions and immunostained with antibodies specific for LMNB1(green) or LMNA/C (green) and for SOX10 (red). DAPI (blue) used as nuclear counterstain. Scale bar, 10 µm.

(D) Scatter plot of the fold change of LMNB1 or LMNA/C protein levels measured by quantifying the relative immunofluorescence in $SOX10^{+}$ immunoreactive cells cultured either in proliferating or differentiating conditions. Data represents average ± SD (n = 3 independent cultures per condition; $p \geq 0.05$, Student's t test two-tailed).

Supplemental figure related to **Figure 1**.

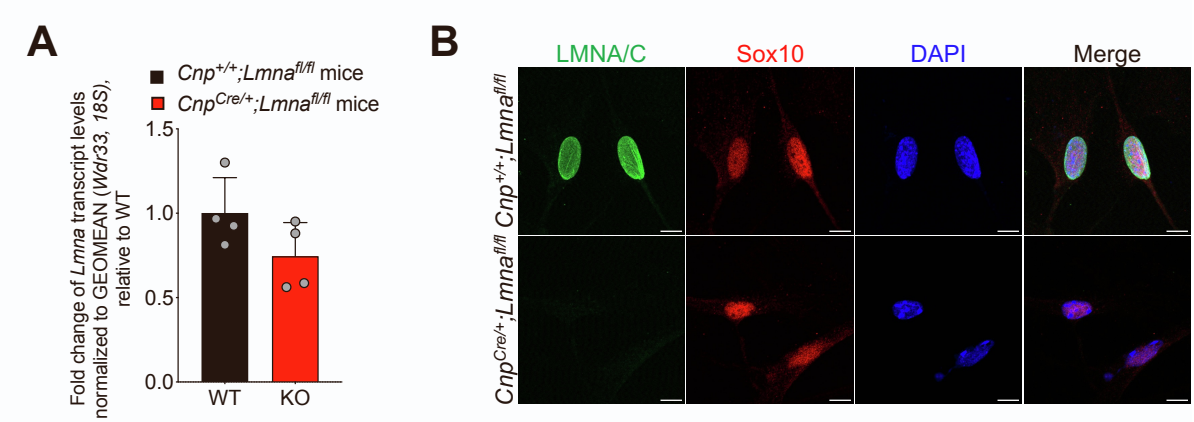

Supplemental Figure S2. Loss of LMNA/C in Schwann cells cultured from *Cnp$^{Cre/+}$;Lmna$^{fl/fl}$* mice.

(A) Scatter plot of *Lmna* transcript levels measured by real-time qPCR in RNA samples extracted from the sciatic nerves of wild type (*Cnp$^{+/+}$;Lmna$^{fl/fl}$*; n =4) and *Lmna* mutant mice (*Cnp$^{Cre/+}$;Lmna$^{fl/fl}$* n = 4; p ≥ 0.05, Student's t test two-tailed).

(B) Representative confocal image of mouse Schwann cells cultured from the sciatic nerves of wild type (*Cnp$^{+/+}$;Lmna$^{fl/fl}$*) and *Lmna* mutant mice (*Cnp$^{Cre/+}$;Lmna$^{fl/fl}$*) and stained for LMNA/C (green) or with SOX10 (red). DAPI (blue) used as nuclear counterstain. Scale bar, 10 μm.

Supplemental figure related to **Figure 3.**

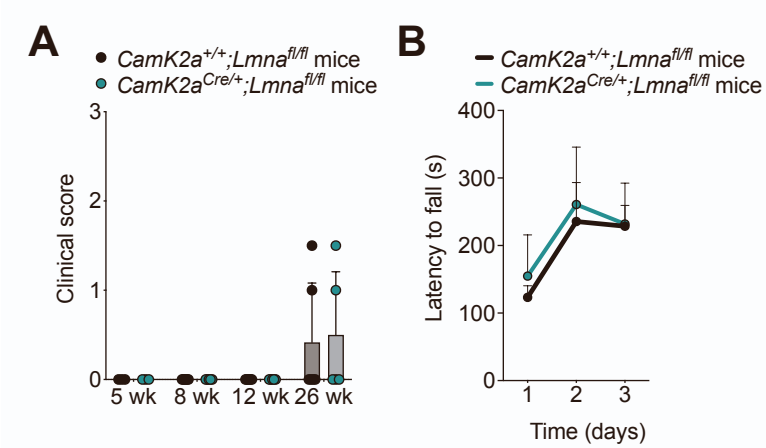

Supplemental Figure S3. Loss of *Lmna* in neurons does not impair mice behavior.
(A) Scatter plot of the clinical score observed in wild type (*CamK2a*$^{+/+}$;*Lmna*$^{fl/fl}$) and *CamK2a*$^{Cre/+}$;*Lmna*$^{fl/fl}$ (cKO) mice at 5 weeks (wk), n = 3 mice per genotype; 8 wk, n = 6 mice per genotype); 12 wk, n = 6 wild type and n = 5 cKO and 26 wk, n = 6 wild type and n = 5 cKO. Data represented as mean + SD ($p \geq 0.05$, two-way ANOVA).
(B) Latency to fall in the rotarod test measured in wildtype (n = 5) and *CamK2a*$^{Cre/+}$;*Lmna*$^{fl/fl}$ mice (n = 4) on 3 consecutive days ($p \geq 0.05$, two-way ANOVA).
Supplemental figure related to **Figure 3.**

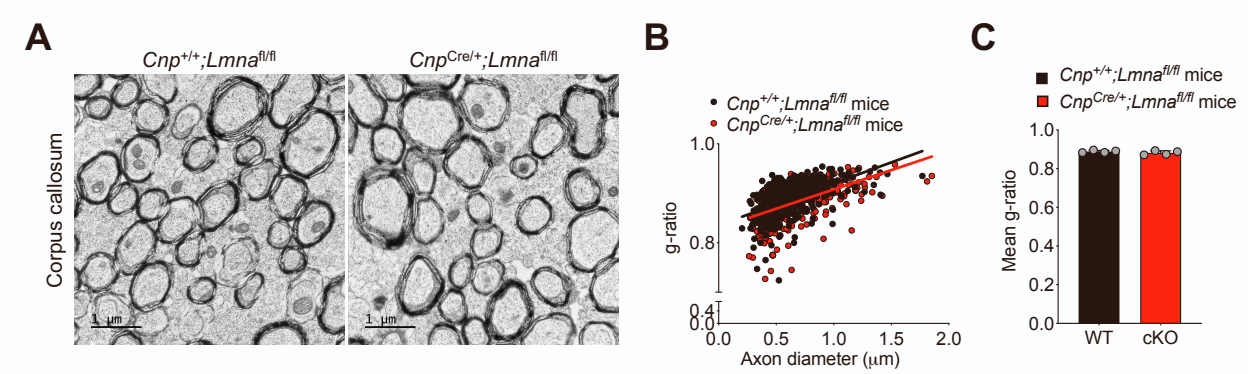

Supplemental Figure S4. Normal myelination profile in *Lmna* young adult mutants.
(A) Representative electron microscopy images of the corpus callosum harvested from 8-week-old control and *Lmna* mutant mice. Scale bar, 1 µm.
(B) Scatter plot of g-ratios relative to the respective axonal diameters in the corpus callosum of 8-week-old control and *Lmna* mutant mice. A total of n = 418 axons in 4 wild type mice and n = 408 axons in 4 *Lmna* mutant mice were measured (WT, slope = 0.0848 ± 0.006, intercept = 0.835 ± 0.004; cKO, slope = 0.078 ± 0.007, intercept = 0.830 ± 0.004).
(C) Scatter plot of average g-ratio values measured in the corpus callosum of 8-week-old control (n = 4) and *Lmna* mutant mice (n = 4). Data represent average ± SD, ($p \geq 0.05$, Student's t test two-tailed).
Supplemental figure related to **Figure 3**.

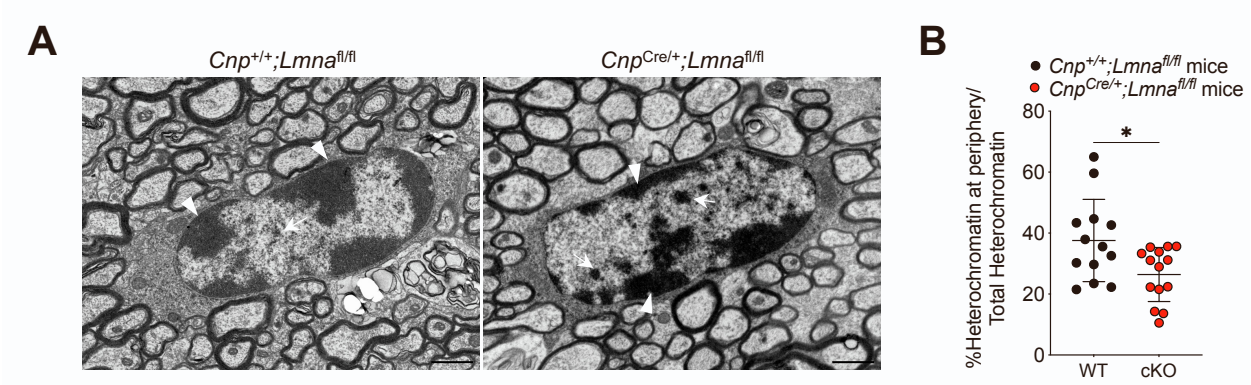

Supplemental Figure S5. Ultrastructural changes in the nuclei of oligodendrocyte lineage cells of *Cnp$^{Cre/+}$;Lmna$^{fl/fl}$* mice.

(A) Representative electron micrographs of nuclei of oligodendrocyte lineage cells in wild type (*Cnp$^{+/+}$;Lmna$^{fl/fl}$*) and *Lmna* mutant (*Cnp$^{Cre/+;}$Lmna$^{fl/fl}$*) mice. White arrowheads indicate heterochromatin at the nuclear periphery; white arrows indicate heterochromatin inside the nuclei. Scale bar, 1 µm.

(B) Scatter plot of the percentage of heterochromatin at the periphery over the total heterochromatin area (n = 13 nuclei in 3 wild type and n = 14 in 3 *Lmna* mutant mice). Data represented as mean ± SD (*p < 0.05, Student's t test two-tailed).

Supplemental figure related to **Figure 4**.

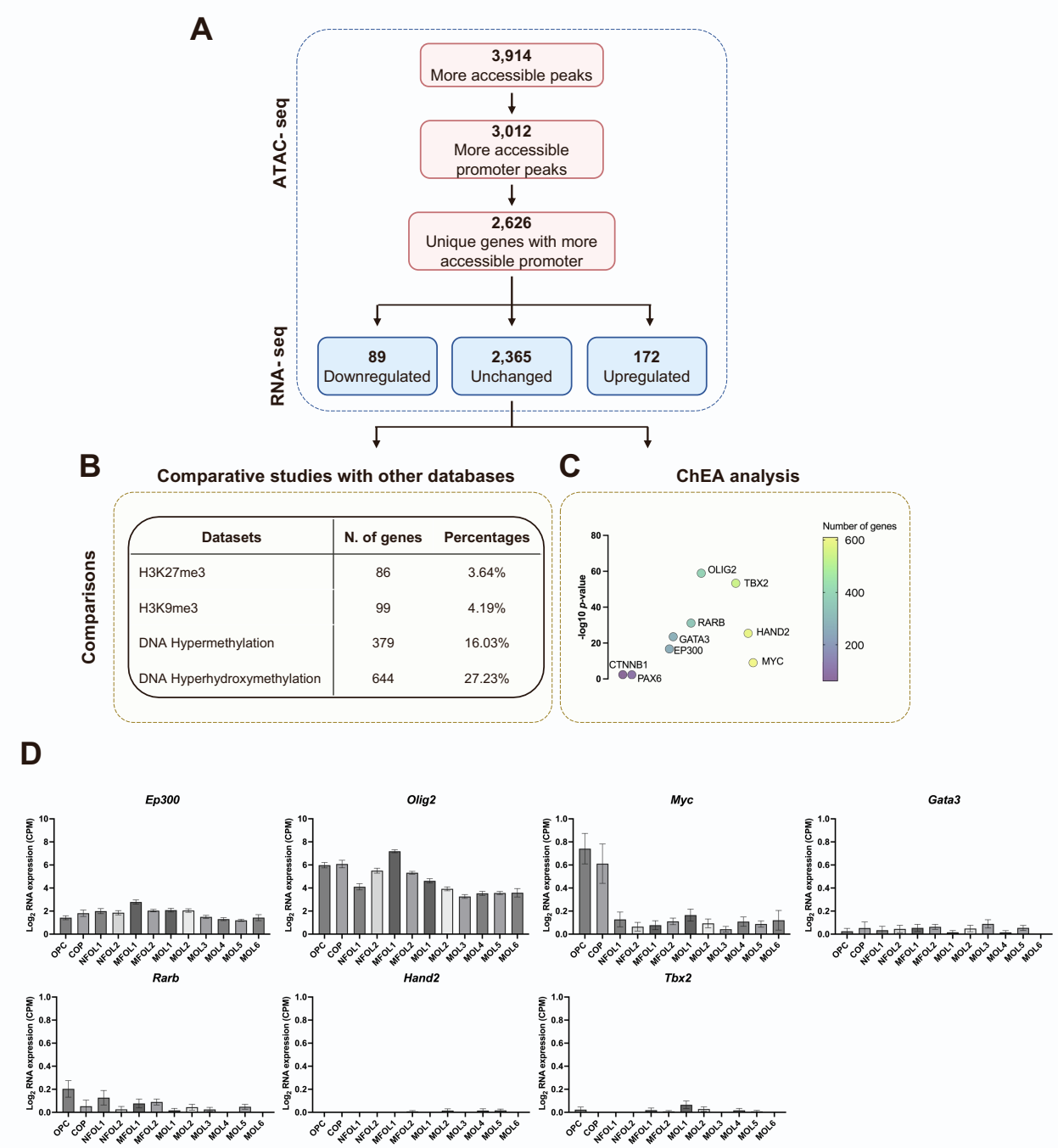

Supplemental Figure S6. Analysis of the ATAC-seq data set identifies transcriptional and epigenetic regulators of the genomic areas with increased chromatin accessibility.

(A) Flowchart representing the analysis conducted on the genes with more accessible chromatin regions in *Lmna* mutant myelinating oligodendrocytes (*Ndrg1-EGFP;Cnp*$^{Cre/+}$*;Lmna*$^{fl/fl}$) compared to controls (*Ndrg1-EGFP;Cnp*$^{+/+}$*;Lmna*$^{fl/fl}$). Genes identified by ATAC-seq characterized by more accessible promoter regions (pink) were overlapped with the RNA-seq datasets (blue) also obtained from the FACS-sorted myelinating oligodendrocytes (mOLs).

(B) The genomic regions corresponding to the 'unchanged' transcripts between the two genotypes were interrogated against previously reported datasets, such as H3K27me3 ChIP-seq (Liu et al., 2015 [S1]) or H3K9me3 ChIP-seq (Liu et al., 2015 [S1]), as well DNA methylation data from Enhanced Reduced Representation Bisulfite Sequencing (ERRBS, Moyon et al., 2016 [S2]) and

DNA hydroxymethylation from Reduced Representation Hydroxy Profiling (RRHP, Moyon et al., 2021 [S3]). The results are shown as gene numbers (referring to genes present in both datasets) as well as percentage relative to the total number of genes with accessible chromatin and unchanged transcript levels.
(C) Chromatin Enrichment Analysis (ChEA) of the same data set, identified validated regulatory transcription factors (TF) in common among all the genes with increased chromatin accessibility and no changes in their transcript levels. The colored circles provide a visual representation of the number of identified gene target for each of the indicated TF.
(D) Bar graphs showing the log_2CPM (counts per million reads mapped) expression levels (Average ± standard error of the mean) of *Ep300*, *Olig2*, *Myc*, *Gata3*, *Rarb*, *Hand2*, and *Tbx2* in oligodendrocyte lineage cells at distinct stages of differentiation, as reported in published dataset (Marques et al., 2016 [S4]). OPC, oligodendrocyte precursor; COP, Differentiation-committed oligodendrocyte precursors; NFOL, newly formed oligodendrocytes; MFOL, Myelin-forming oligodendrocytes; MOL, mature oligodendrocytes.
Supplemental figure related to **Figure 4** and **Figure 5**.

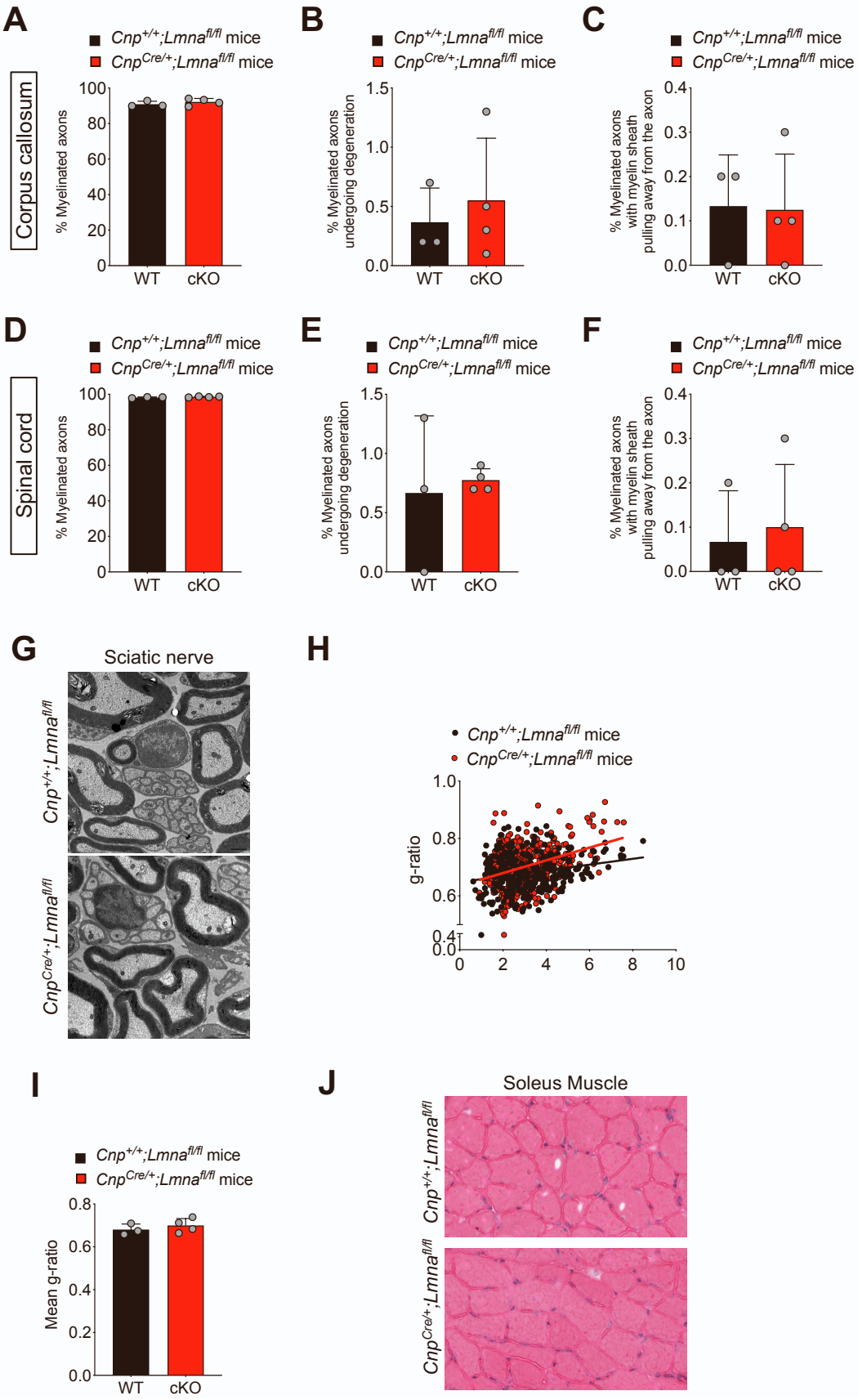
A
B
C
D
E
F
G
H
I
J
Corpus callosum
Spinal cord
Cnp+/+;Lmnafl/fl mice
CnpCre/+;Lmnafl/fl mice
% Myelinated axons
% Myelinated axons undergoing degeneration
% Myelinated axons with myelin sheath pulling away from the axon
WT
cKO
Sciatic nerve
Cnp+/+;Lmnafl/fl
CnpCre/+;Lmnafl/fl
g-ratio
Mean g-ratio
Soleus Muscle

Supplemental Figure S7. Effect of loss of LMNA/C on central myelinated axons and peripheral nerve and muscle.

(A, B, C) Scatter plots of the percentage of myelinated axons (A), myelinated axons undergoing degeneration (B), myelinated axons with the myelin sheath pulling from the axons (C) analyzed from electron micrographs of the corpus callosum of 26-week-old control (n = 3) and *Lmna* mutant (n = 4) mice.

(D, E, F) Scatter plots of the percentage of myelinated axons (D), myelinated axons undergoing degeneration (E), myelinated axons with the myelin sheath pulling from the axons (F) analyzed from electron micrographs of the spinal cord of 26-week-old control (n = 3) and *Lmna* mutant (n = 4) mice.

Data represented as mean ± SD, (A-F), $p \geq 0.05$ Student's t test two-tailed.

(G) Representative electron micrographs of sciatic nerve sections from 26-week-old wild type and *Lmna* mutant mice. Scale bar, 1 μm.

(H) Scatter plot of g-ratios relative to axonal size, in the sciatic nerve of 26-week-old wild type and *Lmna* mutant mice. A total of n = 314 axons in 3 wild type mice and n = 390 axons in 4 *Lmna* mutant mice was measured (WT, slope = 0.0101 ± 0.002, intercept = 0.648 ± 0.008; cKO, slope = 0.0221 ± 0.003, intercept = 0.635 ± 0.0098).

(I) Scatter plot of average values of the g-ratio showing not significant differences between the sciatic nerve of 26-week-old wildtype (n = 3) and *Lmna* mutant mice (n = 4); data represented as mean ± SD ($p \geq 0.05$ Student's t test two-tailed).

(J) Representative image of H&E staining in the soleus muscle of 26-week-old wild type and *Lmna* mutant mice. Scale bar, 50 μm.

Supplemental figure related to **Figure 7**.

Table S1. GO Terms Biological Process and associated genes of transcripts upregulated in mature OLs of *Lmna* mutant mice compared to controls.
Supplemental table related to **Figure 5**.

GO ID	GO Term	Count	%	Pval	-log10(Pval)	Genes
GO:0035556	intracellular signal transduction	38	5.65	4.97E-08	7.30	SIRPB1A, MAST3, PRKCZ, ADCY7, NRBP2, ABR, PREX1, IRAK1, RASSF5, MCF2L, DVL3, SOCS6, SH2B3, PDK1, MAPK3, PEA15A, LYN, UNC13B, MAP4K1, WSB1, NFAM1, MINK1, DEF8, ARHGAP45, MAPK10, DAB1, TAOK3, WNK1, TAOK2, DCX, PTPN6, LCP2, RAPGEF5, SGK2, CILK1, ASB1, RAPGEF4
GO:0016477	cell migration	29	4.29	4.84E-07	6.31	ITGB4, BRAT1, ITGB2, TNFAIP3, LAMC1, RND2, LIMD1, PRKCZ, TREM1, ABR, ADGRG1, CDH2, MYO18A, SIRPA, ITGB7, CTNNA2, PDK1, APC2, PDGFRA, MMP2, RRAS2, GFRA1, L1CAM, MMP9, FMNL1, ELMO2, CORO7, DOCK2, CD44
GO:0007155	cell adhesion	38	5.62	6.24E-05	4.20	CYFIP2, NLGN3, RIPOR2, PTPRS, CSF3R, COL16A1, ITGB4, TTYH1, ZAN, ITGA2B, ITGB2, INPPL1, LAMC1, ITGAL, NID1, THBS3, ADGRG1, CDH2, ADGRE5, EMILIN2, NRCAM, ITGB7, CTNNA2, KIRREL3, PCDH7, L1CAM, SORBS3, NFASC, DAB1, SELL, COL6A2, CDHR2, CNTN1, PMP22, CDH13, SSPO, CD44, JCAD
GO:0008285	negative regulation of cell proliferation	28	4.14	3.75E-04	3.43	DDR1, CDKN1A, NOTCH1, SLFN2, INPPL1, SLC9A3R1, ADGRG1, RASSF5, FNTB, NDN, MFN2, JARID2, SH2B3, TRP53INP1, LYN, SMAD3, TSC1, PROX1, SIRT2, CXCL12, DLC1, PMP22, CDH13, STRN, HSPA1B, GPLD1, HSPA1A, TLR2
GO:0006954	inflammatory response	26	3.85	6.22E-04	3.21	IL25, TRIL, TNFAIP3, PRKCZ, HDAC7, C3, C4B, CCL9, CLEC7A, CCL6, CCL5, ALOX5, CCL4, RIPK1, LYN, HPS1, CYBB, CELA1, LILRB4A, TNFRSF1B, IL17RA, HCK, THEMIS2, SMPDL3B, CD44, TLR2
GO:0030154	cell differentiation	53	7.84	1.39E-03	2.86	RIPOR2, SPI1, TENM4, THRA, TNFAIP2, CLGN, RIMS2, NHSL1, JARID2, MEF2A, SEMA6A, CEP131, NAV1, SIRT2, FGR, HCK, ELF4, CDHR2, DCX, ZFP423, CATSPER2, NOTCH1, SEMA3E, HSD17B7, GATA2, SPATA6, ADGRG1, SBNO2, CTNNA2, SH2B3, CNMD, MEF2D, LYN, SEMA4A, SMAD3, SEMA4D, HSPA1L, SRD5A1, SEMA4F, HSPA2, NR1D1, EIF2AK4, PUM1, L1CAM, PRRC2A, DAB1, BMP1, PMP22, TLL2, SSPO, PTPN6, AGRN
GO:0006914	autophagy	16	2.37	1.46E-03	2.84	RUBCN, TRIM30A, ITGB4, TGFBRAP1, GPR137B, SIRT2, PMP22, ATG2A, MFN2, ATP13A2, HAP1, SBF2, TECPR1, TRP53INP2, VPS16, TRP53INP1
GO:0048008	platelet-derived growth factor receptor signaling pathway	6	0.89	7.04E-03	2.15	PDGFRA, PLEKHA1, SCHIP1, TXNIP, PLAT, PTPN11
GO:0006915	apoptotic process	32	4.73	1.17E-02	1.93	CYFIP2, NOTCH1, BRAT1, AATK, TNFAIP3, LSP1, PPM1F, RASSF5, MFN2, PMAIP1, RIPK1, PHLDA1, MEF2D, RBM5, MAPK3, PEA15A, TRP53INP1, SRGN, MEF2A, CASR, SEMA6A, PDCD6IP, GSN, NSG1, MMP9, NISCH, PACS2, DLC1, MADD, LCN2, ELMO2, TNFRSF21

Table S2. GO Terms Cellular components and associated genes of transcripts downregulated in mature OLs of *Lmna* mutant mice compared to controls.
Supplemental table related to **Figure 5**.

GO ID	GO Term	Count	%	Pval	-log10(Pval)	Genes
GO:0005743	mitochondrial inner membrane	45	8.35	2.63E-12	11.6	CNP, ABCB7, NDUFB5, ATP6, MRPS31, ATP5C1, MRPL15, MRPS30, ATP5H, TMEM70, TMEM242, MRPL20, HMGCL, MRPL40, AIFM1, TMEM65, ATP5E, NAT8F1, TIMM17A, COX3, COX2, PMPCB, COX1, NDUFV2, CHCHD1, MRPS28, GPX4, ATP5PB, BCKDHB, MRPL47, MRPL48, COX6C, SDHB, MRPL21, GCAT, HADHB, NDUFS8, CHDH, NDUFS4, TMEM126A, ND1, CYTB, UQCRC2, ND2, ND4
GO:0005739	mitochondrion	94	17.44	2.14E-10	9.67	NRP1, HIBADH, ATP5C1, ATP5G3, ALKBH7, GJA1, MCEE, MRPL40, HMGN5, AIFM1, DPYSL2, BSG, TIMM17A, PMPCB, CHCHD1, MRPS28, MCCC2, ACOT9, PPTC7, GPX4, BCKDHB, NME2, CTPS2, ACOT13, HAUS3, NME3, MRPL47, MRPL48, ACSL3, SDHB, GCAT, HADHB, FAM210B, NDUFS8, ETHE1, CHDH, NDUFS4, TMEM126A, JTB, ND1, UQCRC2, FKBP4, PFDN4, ND2, PI4K2A, ND4, ABCG2, ECHS1, NAXE, ABCB7, ATP8, NDUFB5, ATP6, MRPS31, MRPL15, MRPS30, MAT2B, ATP5H, HSPA13, TMEM70, TMEM242, PRDX3, MRPL20, HMGCL, PGRMC1, TMEM65, PRDX1, ATP5E, PERP, COX3, STOM, COX2, COX1, NDUFV2, ARGLU1, MCL1, BCAP31, PTCD2, MDH1, MMAA, HSPA5, ATP5PB, PNPLA8, HSPE1, COX6C, ACADSB, MRPL21, YRDC, GOLPH3, SUCLA2, NDUFAB1, ALPL, CYTB, GRSF1
GO:0043209	myelin sheath	22	4.08	1.87E-08	7.73	CAR2, GSTM1, MDH1, HSPA5, CNP, ATP5PB, NME2, ATP5C1, ATP5H, ATP1B1, TUBB4B, SEPTIN7, PRDX3, SUCLA2, DPYSL2, PRDX1, UQCRC2, NDUFV2, PPIA, CCT5, PACSIN1, ARF6
GO:0070469	respiratory chain	17	2.23	3.36E-07	6.47	NDUFS8, NDUFB5, NDUFS4, NDUFAB1, COX2, ND1, COX1, UQCRC2, CYTB, NDUFV2, ND2, ND4
GO:0005576	extracellular region	77	14.29	1.18E-05	4.93	TPSB2, ECM2, RIF1, WFDC2, NPPC, ISLR, EFEMP2, BMPER, CCN5, RSPO3, SOSTDC1, IL12A, CCN3, LBP, TIMP1, PAMR1, CD34, PLA2G12A, ADGRV1, IGFBP5, ANXA2, COL25A1, IGFBP2, EPDR1, RNASE4, ECRG4, IL17RB, PGF, DKK3, TGFBR3, SELENOP, COL6A1, SCG5, COL8A1, FAM20C, DIPK2A, NBL1, PPIA, ANK, NAXE, HTRA3, HTRA1, FBLN1, FSTL1, FBLN5, DPP4, PLAC9, SERPINB1A, VTN, TTR, CCL7, PENK, SPP1, IGFBP6, APOE, A2M, GPC6, CRTAP, GSTM1, NDFIP1, HSPA5, TGFB3, CMA1, GALNT1, CRIM1, VEGFC, PRG4, SERPINA3N, SOD3, BMP6, BMP5, MANF, BMP2, MGP, OGN, CD9, FOLR1
GO:0005783	endoplasmic reticulum	70	12.99	2.10E-05	4.86	RAB9, RPL5, LPGAT1, PIGYL, GJA1, TMEM147, RPL36AL, BSG, NAT8F1, TMEM38B, SREBF1, SCARA3, PTGIS, ABCA8A, ELOVL5, FBXO2, AHSA1, SLC35G1, ACSL3, PDIA6, CKAP4, DPM1, HADHB, TGFBR3, PIGC, CPED1, METTL7A1, PLPP6, SMO, METTL7A2, METTL7A3, FKBP7, FAM20C, PIGF, GRAMD1B, CRABP2, ZDHHC20, HSPA13, DPP4, VTN, PGRMC1, RNF139, SRP54B, STOM, CEPT1, SRP54A, APOE, CYP2F2, KDSR, BCAP31, XBP1, CRTAP, SDF2L1, NDFIP1, HSPA5, PNPLA8, CNBP, TRAPPC4, AMFR, SLC16A11, FMO1, SULF1, MANF, VMP1, RNF145, SPCS1, RNF103, RPS3A1, MGP, RETREG1
GO:0005753	mitochondrial proton-transporting ATP synthase complex	6	1.11	6.19E-05	4.21	ATP8, ATP5PB, ATP5E, ATP6, ATP5C1, ATP5H

Table S3. Demographics of human specimens used for the assessment of LMNA/C and LMNB1 expression.
Supplemental table related to **STAR Methods**.

Gender	Age	Diagnosis
M	20	Epilepsy
M	39	Epilepsy with mesial temporal onset
M	19	Gliotic brain

Table S4. List of real-time qPCR primers. Supplemental table related to **STAR Methods.**

Real-time qPCR primers	**Source**	**Identifier**
Atp5e Fwd: 5'-CAGGCTGGACTCAGCTACATC-3'	Primer Bank	ID: 13385484a1
Atp5e Rev: 5'-GTTCGCTTTGAACTCGGTCTT-3'	Primer Bank	ID: 13385484a1
Cd44 Fwd: 5'-TCGATTTGAATGTAACCTGCCG-3'	Primer Bank	ID: 26337169a1
Cd44 Rev: 5'-CAGTCCGGGAGATACTGTAGC-3'	Primer Bank	ID: 26337169a1
Gapdh Fwd: 5'-ACCCAGAAGACTGTGGATGG-3'	(Moyon et al., 2016)[S2]	N/A
Gapdh Rev: 5'- CACATTGGGGGTAGGAACAC-3'	(Moyon et al., 2016)[S2]	N/A
Lmna (vivo) Fwd: 5'-CCCGCAAGACCCTTGATTCT-3'	This paper	N/A
Lmna (vivo) Rev: 5'-CCAACAAGTCCCCCTCCTTC-3'	This paper	N/A
Lmna (vitro) Fwd: 5'-CAGTGAGAAGCGCACATTGG-3'	This paper	N/A
Lmna (vitro) Rev: 5'-GCCTGTTCTCAGCATCCACT-3'	This paper	N/A
Lmnb1 (vivo) Fwd: 5'-CAGGAATTGGAGGACATGCT-3'	This paper	N/A
Lmnb1 (vivo) Rev: 5'-GTAGGCGCTGATCTCCATGT-3'	This paper	N/A
Lmnb1 (vitro) Fwd: 5'-AGCTCACCGGGCTCAAGGCT-3'	(Yattah et al., 2020)[S5]	N/A
Lmnb1 (vitro) Rev: 5'-AGCAGCAGCTGGTCGTGCTC-3'	(Yattah et al., 2020)[S5]	N/A
Ndufb5 Fwd: 5'- CAAGAGACTGTTTGTCGTCAAGC-3'	This paper	N/A
Ndufb5 Rev: 5'-TGTTCACCAGTGTTATGCCAAT-3'	This paper	N/A
Srebf1 Fwd: 5'-GCAGCCACCATCTAGCCTG-3'	Primer Bank	ID: 14161491a1
Srebf1 Rev: 5'-CAGCAGTGAGTCTGCCTTGAT-3'	Primer Bank	ID: 14161491a1
18S Fwd: 5'-AGTCCCTGCCCTTTGTACACA-3'	(Yattah et al., 2020)[S5]	N/A
18S Rev: 5'-GATCCGAGGGCCTCACTAAAC-3'	(Yattah et al., 2020)[S5]	N/A
Wdr33 Fwd: 5'-TGATCTGGTCCCACCAATAG-3'	(Moyon et al., 2016) [S2]	N/A
Wdr33 Rev: 5'-TGACCAATCGTCTTCCTTCC-3'	(Moyon et al., 2016) [S2]	N/A

REFERENCES

[S1] Liu, J., Magri, L., Zhang, F., Marsh, N.O., Albrecht, S., Huynh, J.L., Kaur, J., Kuhlmann, T., Zhang, W., Slesinger, P.A., et al. (2015). Chromatin landscape defined by repressive histone methylation during oligodendrocyte differentiation. The Journal of Neuroscience: The Official Journal of the Society for Neuroscience *35*, 352–365. 10/f6x53j.

[S2] Moyon, S., Huynh, J.L., Dutta, D., Zhang, F., Ma, D., Yoo, S., Lawrence, R., Wegner, M., John, G.R., Emery, B., et al. (2016). Functional characterization of DNA methylation in the oligodendrocyte lineage. Cell Reports *15*, 748–760. 10/ggtgz8.

[S3] Moyon, S., Frawley, R., Marechal, D., Huang, D., Marshall-Phelps, K.L.H., Kegel, L., Bøstrand, S.M.K., Sadowski, B., Jiang, Y.-H., Lyons, D.A., et al. (2021). TET1-mediated DNA hydroxymethylation regulates adult remyelination in mice. Nat Commun *12*, 3359. 10/gkf6hb.

[S4] Marques, S., Zeisel, A., Codeluppi, S., Van Bruggen, D., Mendanha Falcão, A., Xiao, L., Li, H., Häring, M., Hochgerner, H., Romanov, R.A., et al. (2016). Oligodendrocyte heterogeneity in the mouse juvenile and adult central nervous system. Science *352*, 1326–1329. 10.1126/science.aaf6463.

[S5] Yattah, C., Hernandez, M., Huang, D., Park, H., Liao, W., and Casaccia, P. (2020). Dynamic Lamin B1-Gene Association During Oligodendrocyte Progenitor Differentiation. Neurochem Res *45*, 606–619. 10/gqrhh4.